DOI: 10.1002/zaac.201300271

Molecular Structure and Real-Space Bonding Descriptors (AIM, ELI-D) of Phenyl(triphenylstannyl)telluride

Jens Beckmann,*[a,b] Darina Heinrich,[a] and Stefan Mebs*[a]

Keywords: Tellurium; Tin; Density functional calculations; X-ray diffraction

Abstract. The previously known phenyl(triphenylstannyl)telluride, $PhTeSnPh_3$, was prepared by the reaction of triphenyltin chloride, Ph_3SnCl, with sodium phenyltellurolate, Na(TePh), in liquid ammonia. The molecular structure established by X-ray crystallography and by geometry optimization at the DFT/B3PW91/TZ level of theory was used for calculations of real-space bonding descriptors derived from an atoms-in-molecules (AIM) analysis of the theoretically calculated electron density. In addition, the electron localizability indicator (ELI-D) was derived from the corresponding pair density and the Raub-Jansen-Index (RJI) was determined.

Introduction

Studies involving the nature of chemical bonds are of utmost concern for nearly all branches of chemistry. Small molecules containing bonds between two distinctive p-block elements are useful candidates for detailed bond analyses using real-space bonding descriptors derived from the electron density (ED) and the pair density. We recently reported an in-depth study on σ-donor stabilized aryltellurenyl cations $[MesTe(EPh_3)]^+$ (E = P, As, Sb) and $[MesTe(TeMes_2)]^+$, which are best described as mesityltelluro-substituted triphenylphosponium, triphenylarsonium, triphenylstibonium, and dimesityl telluronium cations, respectively, due to the fact that most of the positive charge is situated at the donor atoms E.[1] Aryl(triphenylstannyl)tellurides Ph_3SnTeR are isoelectronic to aryltelluro-substituted triphenylstibonium cations $[RTeSbPh_3]^+$, but lack a positive charge.

In this study, we extend the bond analysis to the previously known phenyl(triphenylstannyl)telluride, $Ph_3SnTePh$, a simple molecule containing a Sn–Te bond.[2–4] The structural analysis based on X-ray crystallography is supported by density functional theory (DFT) calculations performed at the B3PW91/TZ level of theory. The experimental and theoretically optimized structures are topologically analyzed according to the Atoms-In-Molecules (AIM)[5] and Electron-Localizability-Indicator (ELI-D)[6] space partitioning schemes, respectively. The AIM-approach has found wide applications in the last two decades,[7] however, the ELI-D introduced in 2004 is not yet a standard tool in the field. Besides our own work[1] we are aware of only one other study applying the ELI-D on tellurium compounds.[8]

Results and Discussion

Phenyl(triphenylstannyl)telluride, $Ph_3SnTePh$, has been previously prepared by the reaction of PhTeTePh with Ph_3SnH in yields of 50–70 %[2] and by the reaction of PhTeTePh with $NaBH_4$ and Ph_3SnCl in yields of 76 %,[3] and characterized by Raman, UV, NMR (^{119}Sn, ^{125}Te), and Mößbauer (^{119}Sn, ^{125}Te) spectroscopy.[3,4]

We prepared $Ph_3SnTePh$ by salt metathesis of Ph_3SnCl with NaTePh (generated in situ from PhTeTePh and Na) in liquid ammonia in 78 % yield [Equation (1)]. The melting point (97 °C, lit. 95–97 °C[3]) as well as the ^{119}Sn and ^{125}Te NMR chemical shifts of –127.6 (lit. –125.0[4]) and –202.5 (lit. –205.8[4]) ppm resemble literature values and confirm the authenticity of the material.

$$Ph_3SnCl + NaTePh \xrightarrow[-NaCl]{\text{liquid } NH_3} Ph_3SnTePh \quad (1)$$

The molecular structure of $Ph_3SnTePh$ is shown in Figure 1 and selected bond parameters are collected in the caption of the figure. The spatial arrangement of the tin atom is slightly distorted tetrahedral with the C–Sn–C and C–Sn–Te angles ranging from 108.2(2) to 110.3(2)°.

The Sn–Te–C angle of 90.2(1)° is identical within the experimental error to the Sb–Te–C angle of the $MesTe(SbPh_3)_3]^+$ cation.[1] The Te–Sn bond length of 2.732(1) Å is slightly longer than the Te–Sb bond length of the $[MesTe(SbPh_3)]^+$ cation [2.708(1) Å],[1] which is presumably affected by the positive charge and an additional ionic bond contribution arising thereof. There are no significant intermolecular contacts

* Prof. Dr. J. Beckmann
E-Mail: j.beckmann@uni-bremen.de
* Dr. S. Mebs
E-Mail: stebs@chemie.fu-berlin.de
[a] Institut für Chemie und Biochemie
Freie Universität Berlin
Fabeckstraße 34/36
14195 Berlin, Germany
[b] Institut für Anorganische Chemie
Universität Bremen
Leobener Straße
28359 Bremen, Germany

Supporting information for this article is available on the WWW under **http://dx.doi.org/10.1002/zaac.201300271** or from the author.

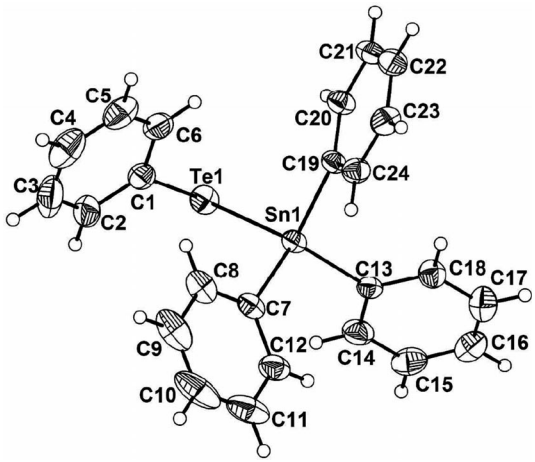

Figure 1. Molecular structure of $Ph_3SnTePh$ showing 30 % probability ellipsoids and the crystallographic numbering scheme. Selected bond parameters /Å,°: Te1–Sn1 2.732(1), Te1–C1 2.134(5), Sn1–C7 2.148(4), Sn1–C13 2.137(4), Sn1–C19 2.137(4), C7–Sn1–Te1 109.8(1), C13–Sn1–Te1 109.2(1), C19–Sn1–Te1 109.8(1), C7–Sn1–C13 110.3(2), C7–Sn1–C19 109.5(2), C13–Sn1–C19 108.2(2), C1–Te1–Sn1 90.2(1). ORTEP representation.[9]

involving the tin and tellurium atoms. Starting from the experimentally obtained atomic coordinates, a geometry optimization was carried out. The superposition of the experimentally and computationally obtained molecular structures is shown in Figure 2. The conformational differences are only marginal, which may justify the sole analysis of the experimental geometry in similar cases when theoretical geometry optimizations may not be feasible due to time constraints.[1]

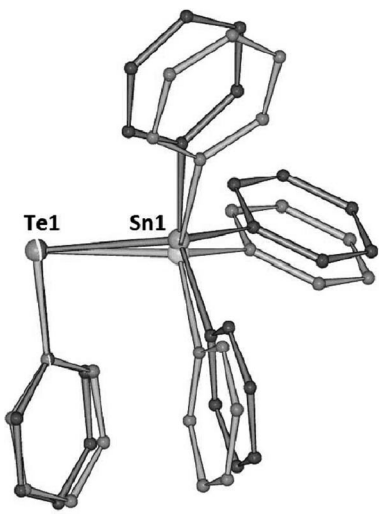

Figure 2. Superposition of the experimentally obtained X-ray structure (light gray) and the computationally optimized gas-phase geometry (dark gray) of $Ph_3SnTePh$. SCHAKAL representation.[10]

The electronic analysis is focused on the Te–Sn, Te–C, and Sn–C bonds and the involved atoms and lone pairs. The bond topology of the experimentally obtained structure of $Ph_3SnTePh$ is shown in Figure 3. The corresponding bond topological parameters are collected in Table 1.

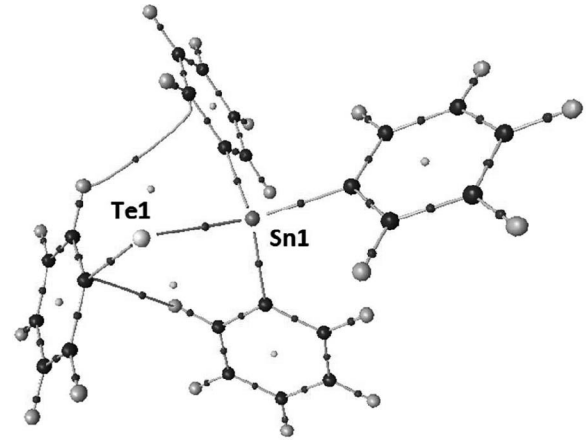

Figure 3. Bond topology in the experimental geometry of $Ph_3SnTePh$. AIM2000 representation.[11]

The ELI-D basin volumes, charges, and attractor values for the Te–Sn, Te–C, and Sn–C bonds and the lone-pair basins of the tellurium atom [Te(LP)] are listed in Table 2. Overall, the results are very similar to those for the previously analyzed $[MesTe(SbPh_3)]^+$ and $[MesTe(TeMes_2)]^+$ cations uncovering all listed bond types as polar-covalent interactions.[1] For the ELI-D bonding basins (so called disynaptic valence basins) also the attractor position relative to the atom–atom line and the Raub-Jansen-Index are displayed.[12] The latter is a combination of the AIM and ELI-D partitioning schemes: It quantifies the partial electron numbers of a ELI-D bonding basin within the bond contributing AIM atoms. The RJI is 50 % for homopolar bonds and increases for polar interactions. Dative bonds are represented by an RJI of at least 95 %.[13] The ELI-D is displayed for two different iso values in Figure 4. At Y = 1.4 the Te–Sn basin is not visible as the ELI-D value at the attractor position is 1.34. The bonding electrons are much less localized in the Te–Sn interaction than in the Te/Sn–C bonds, which is reflected in the small value for the ED at the bond critical point (bcp), the larger bond ellipticity (ε), the smaller curvature along the bond path (λ_3), the smaller localizability value at the ELI-D attractor position of the Te–Sn basin (Y_{max}) and the larger distance of the ELI-D attractor position to the atom–atom line (d_{ELI}).

The smaller difference of the electronegativity between tellurium and tin compared to Te/Sn–C is reflected in the Laplacian being close to zero (instead of being significantly positive), a smaller interpenetration of the tellurium and the tin atom compared to Te/Sn and C, which gives rise to a smaller $G/\rho(\mathbf{r})_{bcp}$ value for Te–Sn and a Raub-Jansen-Index (RJI) close to 50 %. With 1.55 e the electron population in the Te–Sn basin is significantly smaller than in the related compounds comprising Te–*E* (*E* = P, As, Sb) bonds (1.89–1.95 e) and comparable to the Te–Te bond (1.61 e) of the $[MesTe(TeMes_2)]^+$ cation.[1] However, the ELI-D value at the attractor position, Y_{max} = 1.34, is similar to the Te–Sb bond (1.32) and the Te–Te bond (1.36) of the $[MesTe(SbPh_3)]^+$ and $MesTe(TeMes_2)]^+$ cations.[1] Integration of the electron population within the AIM basins leads to AIM-atomic volumes and charges. Summing

Zeitschrift für anorganische und allgemeine Chemie ZAAC Journal of Inorganic and General Chemistry

Table 1. Bond topological properties[a] of the Te–Sn, Te–C, and Sn–C bonds of $Ph_3SnTePh$. First row: values at experimentally obtained geometry, second row (*italics*): values at computationally optimized gas-phase structure.

Bond	d /Å	$\rho(\mathbf{r})_{bcp}$ /e•Å^{-3}	$\Delta\rho(\mathbf{r})_{bcp}$ /e•Å^{-5}	d_1 /Å	d_2 /Å	ε	λ_3 /e•Å^{-5}	$G/\rho(\mathbf{r})_{bcp}$ /he^{-1}	$H/\rho(\mathbf{r})_{bcp}$ /he^{-1}
Te1–Sn1	2.733	0.45	0.2	1.462	1.271	0.15	2.53	0.37	–0.34
	2.760	*0.43*	*0.2*	*1.476*	*1.284*	*0.16*	*2.40*	*0.35*	*–0.33*
Te1–C1	2.135	0.80	–0.2	1.098	1.037	0.05	5.76	0.50	–0.51
	2.134	*0.80*	*0.0*	*1.097*	*1.037*	*0.03*	*5.80*	*0.50*	*–0.51*
Sn1–C9	2.147	0.72	2.6	1.090	1.057	0.07	8.15	0.68	–0.43
	2.149	*0.72*	*2.7*	*1.090*	*1.059*	*0.07*	*8.18*	*0.69*	*–0.43*
Sn1–C15	2.136	0.73	2.9	1.084	1.052	0.06	8.50	0.71	–0.43
	2.150	*0.71*	*2.7*	*1.090*	*1.060*	*0.06*	*8.17*	*0.69*	*–0.43*
Sn1–C21	2.137	0.73	2.9	1.084	1.053	0.06	8.55	0.71	–0.43
	2.153	*0.71*	*2.9*	*1.091*	*1.062*	*0.06*	*8.14*	*0.69*	*–0.42*

a) For all bonds, $\rho(\mathbf{r})_{bcp}$ is the electron density at the bond critical point, $\Delta\rho(\mathbf{r})_{bcp}$ is the corresponding Laplacian, d_1 and d_2 are the distances from the atom to the bond critical point, ε is the bond ellipticity ($\varepsilon = \lambda_1 / \lambda_2 - 1$; $\lambda_{1/2}$: curvatures perpendicular to the bond path), λ_3 is the curvature along the bond path, $G/\rho(\mathbf{r})_{bcp}$ and $H/\rho(\mathbf{r})_{bcp}$ are the kinetic and total energy density over $\rho(\mathbf{r})_{bcp}$ ratios. Results obtained by an analysis of the wavefunction files with AIM2000.[11]

Table 2. Topological and integrated ELI-D properties[a] of $Ph_3SnTePh$. First row: values at experimentally obtained geometry, second row (*italics*): values at computationally optimized gas-phase structure.

Basin	$V(001)_{ELI}$ /Å^3	$N(001)_{ELI}$ /e	Y_{max}	d_{ELI} /Å	RJI /%
Te–Sn	6.9	1.55	1.34	0.375	53
	7.3	*1.55*	*1.34*	*0.256*	*54*
Te(LP1)	21.0	2.43	1.74	–	–
	21.1	*2.43*	*1.74*	–	–
Te(LP2)	21.7	2.45	1.75	–	–
	21.6	*2.45*	*1.76*	–	–
Te–C1	4.6	1.85	1.67	0.019	72
	4.7	*1.87*	*1.67*	*0.025*	*72*
Sn–C7	9.7	2.27	1.73	0.012	72
	10.0	*2.29*	*1.74*	*0.013*	*73*
Sn–C13	9.7	2.28	1.74	0.019	73
	10.0	*2.29*	*1.74*	*0.007*	*73*
Sn–C19	9.5	2.29	1.74	0.023	74
	10.1	*2.29*	*1.74*	*0.011*	*73*

a) For all basins, $V(001)_{ELI}$ is the basin volume cut at 0.001 a.u., $N(001)_{ELI}$ is the corresponding electron population in that volume, Y_{max} is the ELI-D value at the attractor position, d_{ELI} is the perpendicular distance of the attractor position to the atom–atom line, RJI is the Raub-Jansen-Index (percental electron population within the AIM atom, which has the larger electronegativity). Results obtained by analysis of grid-files using DGRID-4.5.[20]

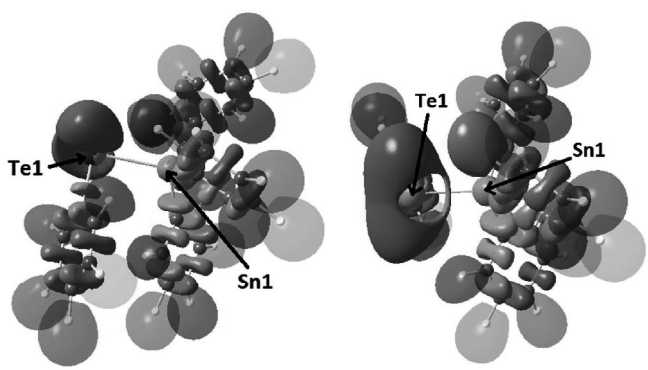

Figure 4. Left side: Side-view ELI-D representation of the experimental X-ray structure of $Ph_3SnTePh$ (Y = 1.4) Small basins are light gray and solid, larger basins are increasingly dark gray and transparent. Right side: corresponding top view at Y = 1.3. The Te–Sn bonding basin is also visible at this iso value. MOLISO representation.[14]

up atomic charges according to functional groups allows for an analysis of electronic substituent effects. In this work, the AIM-charges are analyzed for the experimentally obtained structure of $Ph_3SnTePh$.

The molecular structure is divided into its functional fragments: the tellurium atom (0.01 e), the phenyl ring attached to the tellurium atom (–0.26 e), the tin atom (1.39 e) and the three phenyl rings attached to the tin atom (–0.37 e, –0.38 e, –0.39 e). The relative distribution of charges in $Ph_3SnTePh$ is comparable to the distribution in the $[MesTe(SbPh_3)]^+$ cation: Te = 0.26 e, Ph(Te) = –0.09 e, Sb = 1.39 e, Ph(Sb) = –0.18 each.[1] Thus, the positive charge in the $[MesTe(SbPh_3)]^+$ cation is quite equally distributed over all functional parts of the molecule. According to the electronic real-space bonding properties the bond polarity of the Te–Sn interaction is lower than the Te–P, Te–As, Te–Sb bonds of the $[MesTe(EPh_3)_3]^+$ cations (E = P, As, Sb) and even the Te–Te bond in the $[MesTeTeMes_2]^+$ cation.[1] The same trend is found for the electron localization between the tellurium and the tin atom, which is lower than the cationic reference compounds.

The Sn–Te bond in $Ph_3SnTePh$ was investigated using real-space bonding descriptors derived from an atoms-in-molecules

(AIM) analysis of the theoretically calculated electron density. Moreover, the electron localizability indicator (ELI-D) was derived from the corresponding pair density and the Raub-Jansen-Index (RJI) was determined. Unlike the strongly polar Te–Te and Te–*E* bonds (*E* = P, As, Sb) of the previously reported σ-donor stabilized aryltellurenyl cations $[MesTe(TeMes_2)]^+$ and $[MesTe(EPh_3)]^+$,[1] the Sn–Te bond of $Ph_3SnTePh$ that is rather apolar. The structural differences of molecular structures obtained experimentally by X-ray crystallography and computationally by geometry optimization were only marginally and consequently the analyses of the real-space bonding descriptors gave very similar results.

Experimental Section

The starting materials Ph_3SnCl and PhTeTePh were commercial products and used as received. For general information refer to our preceding paper.[1]

Synthesis of $Ph_3SnTePh$: A flame-dried Schlenk tube was charged with PhTeTePh (230 mg, 0.562 mmol) and cooled to –78 °C before NH_3 (30 mL) was condensed on. To the dark red solution, sodium metal (34.1 mg, 1.48 mmol) was added, which caused a color change to orange. After the mixture was stirred for 2 h, Ph_3SnCl (393 mg, 1.12 mmol) was added and a colorless suspension was formed. The mixture was allowed to warm up to room temperature, while the NH_3 slowly evaporated. The solid residue was extracted with THF (2 × 10 mL) and filtered. The slightly orange filtrate was evaporated to dryness and the crude product was recrystallized from CH_2Cl_2/hexane to give colorless crystals of $Ph_3SnTePh$ (486 mg, 0.88 mmol, 78 %).

X-ray Crystallography: Intensity data were collected with a STOE IPDS 2T area detector fitted with graphite-monochromated Mo-K_α (0.7107 Å) radiation. The structure was solved by direct methods and refined based on F^2 using OLEX2.[15] All non-hydrogen atoms were refined using anisotropic displacement parameters. Hydrogen atoms attached to carbon atoms were included in geometrically calculated positions using a riding model. Crystal and refinement data are collected in Table 3.

Crystallographic data (excluding structure factors) for the structure in this paper have been deposited with the Cambridge Crystallographic Data Centre, CCDC, 12 Union Road, Cambridge CB21EZ, UK. Copies of the data can be obtained free of charge on quoting the depository number CCDC-940870 (Fax: +44-1223-336-033; E-Mail: deposit@ccdc.cam.ac.uk, http://www.ccdc.cam.ac.uk).

Computational Methodology: The experimentally obtained atomic coordinates were taken for a single point calculation and for the geometry optimization applying the DFT functional B3PW91[16] using the program package Gaussian09.[17] The stationary point was characterized as true minimum by a frequency analysis.

For Te and Sn an ECP28MDF electron core potential and the appropriate cc-pVTZ basis set were applied, for all other atoms the 6-311+G(2df,p) basis set was used.[18] C–H distances of all substances were set to neutron diffraction data (C_{sp2}–H 1.083 Å) prior to processing.[19] For the Atoms In Molecules (AIM) analyses, wavefunction files were generated along with the single point calculations and analyzed using AIM2000.[11] DGrid was used to analyze the ELI-D revealing the integrated bond descriptors using a 0.04 a.u. Grid and a 6.0 a.u. box around the molecule.[20]

Table 3. Crystal data and structure refinement of $Ph_3SnTePh$.

Formula	$C_{24}H_{20}SnTe$
Formula weight /g·mol^{-1}	554.69
Crystal system	monoclinic
Crystal size, mm	0.70 × 0.60 × 0.50
Space group	$P2_1/c$
a /Å	12.951(4)
b /Å	9.434(4)
c /Å	18.433(7)
α /°	90.00
β /°	106.09(3)
γ /°	90.00
V /Å^3	2163.9(14)
Z	4
ρ_{calcd} /mg·m^{-3}	1.703
T /K	173
μ (Mo K_α) /mm^{-1}	2.506
$F(000)$	1064
θ range /°	2.30 to 29.21
Index ranges	$-17 \le h \le 11$ $-12 \le k \le 10$ $-25 \le l \le 25$
No. of reflns collected	13160
Completeness to θ_{max}	97.2 %
No. indep. reflections	5700
No. obsd reflns with $[I > 2\sigma(I)]$	4494
No. refined parameters	236
GooF (F^2)	1.013
R_{int}	0.108
R_1 (F) $[I > 2\sigma(I)]$	0.0424
wR_2 (F^2) (all data)	0.1238
$(\Delta/\sigma)_{max}$	< 0.001
Largest diff peak/hole /e·Å^{-3}	0.927 / –1.503

Supporting Information (see footnote on the first page of this article): Cartesian coordinates of the optimized gas-phase structure of $Ph_3SnTePh$.

Acknowledgements

The Deutsche Forschungsgemeinschaft (DFG) is gratefully acknowledged for financial support.

References

[1] J. Beckmann, J. Bolsinger, A. Duthie, P. Finke, E. Lork, C. Lüdtke, O. Mallow, S. Mebs, *Inorg. Chem.* **2012**, *51*, 12395–12406.
[2] N. S. Dance, W. R. McWhinnie, *J. Organomet. Chem.* **1977**, *125*, 291–302.
[3] S. A. Gardner, P. J. Trotter, H. J. Gysling, *J. Organomet. Chem.* **1981**, *212*, 35–42.
[4] C. H. W. Jones, R. D. Sharma, S. P. Taneja, *Can. J. Chem.* **1986**, *64*, 980–986.
[5] R. F. W. Bader Atoms in Molecules. A Quantum Theory; Cambridge University Press, Oxford U. K., **1991**.
[6] M. Kohout, *Int. J. Quantum Chem.* **2004**, *97*, 651–658.
[7] a) T. Koritsanszky, P. Coppens, *Chem. Rev.* **2001**, *101*, 1583–1628; b) C. Gatti, *Z. Kristallogr.* **2005**, *220*, 399–457.
[8] A. Günther, M. Heise, F. R. Wagner, M. Ruck, *Angew. Chem.* **2011**, *123*, 10163–10167.
[9] M. N. Burnett, C. K. Johnson, *ORTEP-III*, Oak Ridge Thermal Ellipsoid Plotting Program for Crystal Structure Illustrations. Report ORNL-6895; Oak Ridge National Laboratory: Tennessee, TN, **1996**.

[10] E. Keller, J.-S. Pierrard, *SCHAKAL99*, A Fortran Program for the Graphical Representation of Molecular and Solid-State Structure Models, Albert Ludwigs Universität Freiburg, Germany, **1999**.
[11] F. Biegler-König, J. Schönbohm, D. Bayles, *AIM2000*, A Program to Analyse and Visualize Atoms, *J. Comp. Chem.* **2001**, *22*, 545–559.
[12] S. Raub, G. Jansen, *Theor. Chem. Acc.* **2001**, *106*, 223–232.
[13] S. Mebs, S. Grabowsky, D. Förster, R. Kickbusch, M. Hartl, L. L. Daemen, W. Morgenroth, P. Luger, B. Paulus, D. Lentz, *J. Phys. Chem. A* **2010**, *114*, 10185–10196.
[14] C. B. Hübschle, P. Luger, *J. Appl. Crystallogr.* **2006**, *39*, 901–904.
[15] O. V. Dolomanov, L. J. Bourhis, R. J. Gildea, J. A. K. Howard, H. Puschmann, *J. Appl. Crystallogr.* **2009**, *42*, 339–341.
[16] a) J. P. Perdew, J. A. Chevary, S. H. Vosko, K. A. Jackson, M. R. Pederson, D. J. Singh, C. Fiolhais, *Phys. Rev. B* **1992**, *46*, 6671–6687; b) A. D. Becke, *J. Chem. Phys.* **1993**, *98*, 5648–5652.
[17] M. J. Frisch, G. W. Trucks, H. B. Schlegel, G. E. Scuseria, M. A. Robb, J. R. Cheeseman, G. Scalmani, V. Barone, B. Mennucci, G. A. Petersson, H. Nakatsuji, M. Caricato, X. Li, H. P. Hratchian, A. F. Izmaylov, J. Bloino, G. Zheng, J. L. Sonnenberg, M. Hada, M. Ehara, K. Toyota, R. Fukuda, J. Hasegawa, M. Ishida, T. Nakajima, Y. Honda, O. Kitao, H. Nakai, T. Vreven, J. A. Montgomery Jr., J. E. Peralta, F. Ogliaro, M. Bearpark, J. J. Heyd, E. Brothers, K. N. Kudin, V. N. Staroverov, R. Kobayashi, J. Normand, K. Raghavachari, A. Rendell, J. C. Burant, S. S. Iyengar, J. Tomasi, M. Cossi, N. Rega, J. M. Millam, M. Klene, J. E. Knox, J. B. Cross, V. Bakken, C. Adamo, J. Jaramillo, R. Gomperts, R. E. Stratmann, O. Yazyev, A. J. Austin, R. Cammi, C. Pomelli, J. W. Ochterski, R. L. Martin, K. Morokuma, V. G. Zakrzewski, G. A. Voth, P. Salvador, J. J. Dannenberg, S. Dapprich, A. D. Daniels, Ö. Farkas, J. B. Foresman, J. V. Ortiz, J. Cioslowski and D. J. Fox *Gaussian 09*, Revision B.01, Gaussian, Inc., Wallingford CT, **2009**.
[18] a) K. A. Peterson, D. Figgen, E. Goll, H. Stoll, M. Dolg, *J. Chem. Phys.* **2003**, *119*, 11113–11123; b) B. Metz, H. Stoll, M. Dolg, *J. Chem. Phys.* **2000**, *113*, 2563–2569; c) K. A. Peterson, *J. Chem. Phys.* **2003**, *119*, 11099–11112.
[19] A. J. C. Wilson, *International Tables of Crystallography*, Kluwer Academic Publishers, Boston, **1992**, vol. C.
[20] M. Kohout, *DGRID*, version 4.5, Radebeul, **2009**.

Received: June 4, 2013
Published Online: August 15, 2013

